EVALUATION ON ULTRASONIC WELDING BEHAVIOR OF CF/PPS AND HEALTH MONITORING USING CNT ADDED ENERGY DIRECTOR

Soma. Nishimura[1], Daiki. Tanabe[2] and Kazuaki. Nishiyabu[3]

[1] Graduate School of Engineering., Osaka University, 2-1, Yamadaoka, Suita city, Osaka 565-0871, Japan, nishimura-s23@mit.eng.osaka-u.ac.jp
[2] Department of Mechanical Eng., Kobe City College of Technology ,8-3, Gakuen-Higashimachi, Nishi-ku, Kobe 651-2194, Japan, kcct-tanabe@g.kobe-kosen.ac.jp
[3] Faculty of Science and Engineering., Kindai University, 3-4-1, Kowakae, Higashiosaka city, Osaka 577-8502, Japan, nishiyabu@mech.kindai.ac.jp

Keywords: CFRTP, Ultrasonic welding, CNT, Welding behavior, Structural health monitoring

ABSTRACT

This study aims to development the ultrasonic welding process using carbon nanotube (CNT) added energy director to reveal the ultrasonic welding behavior, tensile shear strength and damage monitoring of carbon fiber reinforced thermoplastics (CFRTP). The materials used for ultrasonic welding was woven carbon fiber reinforced poly-phenylene sulfide (woven-CF/PPS) or unidirectional carbon fiber reinforced poly-phenylene sulfide laminates (UD-CF/PPS) and energy director consisting of single-walled carbon nanotube (SWCNT), multi-walled carbon nanotube (MWCNT) and PPS polymer. The welding part was evaluated by single lap tensile shear test, image analysis and microscopic observation using scanning electron microscope. Moreover, the electric resistance changing rate ($\Delta R/R$) of welding part under tensile loading was measured for health monitoring. The experimental results revealed that the ultrasonic oscillation time and CNT in the energy director were significantly affected the ultrasonic welding behavior. According to the results of the single lap shear strength test indicate that the addition of CNTs increases the actual tensile shear strength due to nano-fiber reinforcement. Structural health monitoring indicated that the resistance change increased rapidly just before fracture, suggesting the possibility of predicting fracture.

1 INTRODUCTION

Carbon fiber reinforced thermoplastic (CFRTP) are attracting attention recently in aircraft, automotive and industrial applications [1]. A joining technology is necessary for the manufacturing process of CFRTP structures. The ultrasonic welding has some advantages such as very short welding time, low power consumption and ease of automation. The ultrasonic welding parameters for CFRTP such as oscillation time, ultrasonic power, and displacement of the sonotrode has been investigated to optimize the welding conditions [2-4]. Consequently, the method has been proposed in which an energy director made of thermoplastics is inserted into the welding interface [2]. However, the energy director can affect the joining strength and reliability because it remains at the welding interface. The shape and material of the energy director can affect the amount of heat generation and joining strength. Related study on welding technologies for CFRTP is mostly limited to heating element design, mechanical performance of joining part, welding parameters and weld quality. Therefore, it is expected that functionality such as damage monitoring of welding part will be added to welding parts. In damage monitoring, conductive fillers such as CNTs are added to investigate the resistance strain characteristics of welded joints due to the piezoelectric effect [5-9]. This approach may provide a more convenient method for evaluating the structural health monitoring of welded part compared to conventional methods, such as Fiber Bragg Grating (FBG) sensor, ultrasound, thermography and eddy current, different X-ray methods [10]. This study aims to development the ultrasonic welding process using carbon nanotube (CNT) added energy director to reveal the ultrasonic welding behavior, tensile shear strength and damage monitoring of welding part.

2 MATERIALS AND EXPERIMENTAL PROCEDURE

2.1 Materials

The material used for experiment was woven carbon fiber reinforced polyphenylene sulfide laminates (TenCate, CETEX®, woven-CF/PPS). This laminate has 5H satin wave construction with a polymer content of V_f=45 vol.%, thickness of t=2.5 mm, and stacking sequence $[0/90]_8$. The adherends were cut into shapes 20 mm wide and 60 mm long using a wet cutting machine. The energy director was used PPS powder (Toray, TORELINA®, particle diameter 100-300 μm) obtained by crushing frozen PPS pellets as shown in Fig.1(a), single-walled carbon nanotube (OCSiAl, TUBALL™, diameter 1.2-2.0 nm, length 5 μm or more, SWCNT) as shown in Fig.1(b), and multi-walled carbon nanotube (FUJIFILM Wako Pure Chemical Co., Ltd., Diameter 10-30 nm, length 1-10 μm, MWCNT) as shown in Fig.1(c).

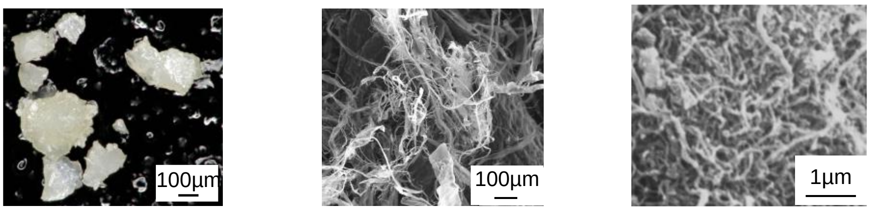

(a) PPS powder (b) SWCNT (c) MWCNT

Figure 1: Microscopic images of (a)PPS powder, (b)single-walled carbon nanotube (SWCNT) and (c)multi-walled carbon nanotube (MWCNT) for energy director. CNT are bundled due to their high cohesive strength.

2.2 Manufacturing process of energy director

Fig.2 shows the manufacturing process of CNT added energy director. This process is mainly divided into four steps. (a) SWCNT or MWCNT were added to PPS powder at an arbitrary weight ratio and dispersed in NMP solvent by ultrasonic vibration, (b) Melt-kneading was performed by using single shaft kneader at 320°C, and (c) The melt-kneaded pellets were molded in vacuum in hot press at 290°C, and 1.5ton for 10 min, which finally resulted in a nominal thickness of 0.2 mm. (d) Finally, the energy director was cut into 25 mm wide and 25 mm long.

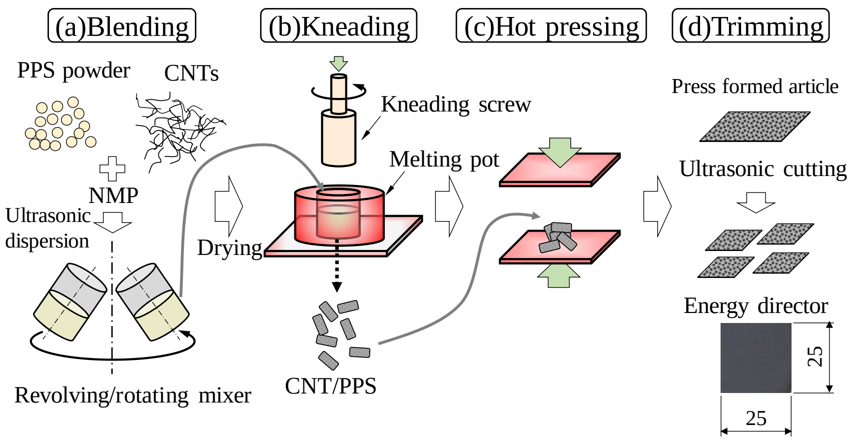

Figure 2: Manufacturing process of CNT added energy director. This process is mainly divided into four steps. (a) CNT were added to PPS powder at an arbitrary weight ratio and dispersed in NMP solvent by ultrasonic vibration, (b) Melt-kneading was performed by using single shaft kneader at 320°C, and (c) The melt-kneaded pellets were molded in vacuum in hot press at 290°C, and 1.5ton for 10 min, which finally resulted in a nominal thickness of 0.2 mm. (d) The energy director was cut into 25 mm wide and 25 mm long using an ultrasonic cutter.

2.3 Ultrasonic welding method

A schematic drawing of the ultrasonic welding equipment is shown in Fig.3. The ultrasonic vibration is generated by applying the ultrasonic output from an ultrasonic oscillator (DUKANE, iQ-Aim®, maximum output power 2600W, frequency 20kHz) to a bolt tightening Langevin-type oscillator, which generates a small amplitude. The ultrasonic vibration was amplified by an ultrasonic horn (horn tip dimension, 27mm×27mm). The ultrasonic vibration was applied with an arbitrary load using a servo press system (Daiichi-Dentsu Co., Ltd., DSP 3000). The energy director generated heat above the melting temperature of PPS polymer (T_m=290°C) due to friction and viscous damping, and the polymer near the fusion welding surface was heated and melted. After that, the polymer was cooled to lower than the glass transition temperature of PPS polymer (T_g=90°C) by air cooling under pressure, and ultrasonic welding was performed by solidifying the polymer.

2.4 Evaluation method

During the ultrasonic welding process, the thickness of the joint decreases due to melting of the polymer. In this study, the rate of decrease in the thickness of the joint was calculated by measuring the distance traveled by the ultrasonic horn as shown in Fig.4. From preliminary experiments, the appropriate horn travel was calculated and applied.

Moreover, single lap shear strength tests were carried out to evaluate the mechanical performance of the welded joints using various CNT added energy director. The schematic drawing of single lap shear specimens was shown in Fig.5 (a). In the joint strength test, three specimens were made under every condition. A universal testing machine (Shimadzu, AG-Xplus 100kN) was used to joining test, and all the test procedures were operated at v=0.5 mm/min cross-head speed. The single lap shear strength was calculated by using this equation:

$$\tau = \frac{P_{max}}{A_w} \tag{1}$$

where τ, single lap shear strength [MPa]; A_w, overlap area [mm^2] and P_{max}, maximum tensile force. Finally, the fracture surfaces of the welded joints were assessed with a microscope (Keyence Co., Ltd., VHX-2000) and scanning electron microscope (JEOL Ltd., JSM-IT200). In addition, to evaluate the degree of resin melting at the welding part, the melted area A_w [mm^2] was calculated from the observed fracture surface image using image analysis software (ImageJ) as shown in Eq. (2), and the ratio divided by the joint area A [mm^2] was evaluated as the melted area ratio ΔA_w [%].

$$\Delta A_w = \frac{A_w}{A} \times 100 \tag{2}$$

Structural health monitoring test was performed via electrical change method of CFRP. Fig.5(b) shows the schematic drawing of health monitoring specimens. The electrodes were formed on the surface of CF/PPS laminate using silver paste. The electric resistance changing rate ($\Delta R/R$) of welding part under tensile loading was measured by using a digital multimeter (ADCMT, 7352A). To quantitatively evaluate the dispersion of CNT and the applicability of self-sensing, the volume resistivity ρ_v[Ω·cm] was measured using a four-point probe method (Fig.6) with a resistivity meter (Nittoseiko Analytech Co., Ltd., Loresta AX, MCP-T370). To measure the electrical volume resistivity, a commonly employed technique involves placing four-point probes in a collinear configuration with equal spacing on the sample. The current is passed through the outer probes, while the voltage is measured between the inner probes. This method eliminates errors associated with electrical contacts since the current and voltage leads are separate. It is widely utilized for measuring volume resistivity. The volume resistivity was calculated by using this equation:

$$\rho_v = \frac{V}{I} \times \frac{1}{t} \times RCF \tag{3}$$

where ρ_v, volume resistivity [Ω·cm]; V, voltage [V]; I, current [A]; t, thickness [cm] and RCF, resistivity correction factor. RCF takes the size of the test specimen, the thickness of the material, the size of the electrodes, and the position of the electrodes with respect to the boundary of the test specimen into account.

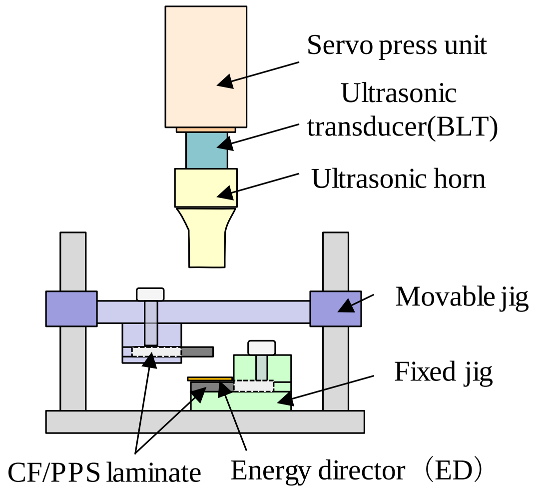

Figure 3: Schematic diagram of ultrasonic welding device

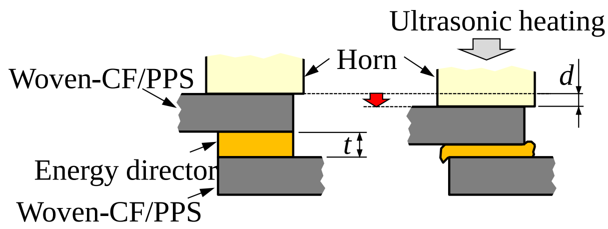

Figure 4: Horn travel distance by ultrasonic welding.

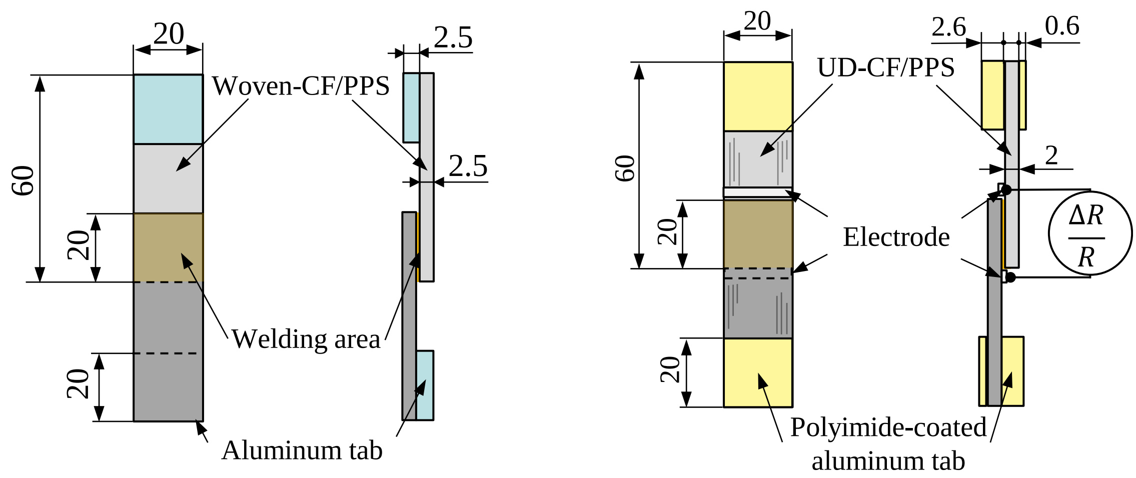

(a)For single lap shear test

(b)For structural health monitoring evaluation

Figure 5: Geometry of single lap tensile shear test specimens.

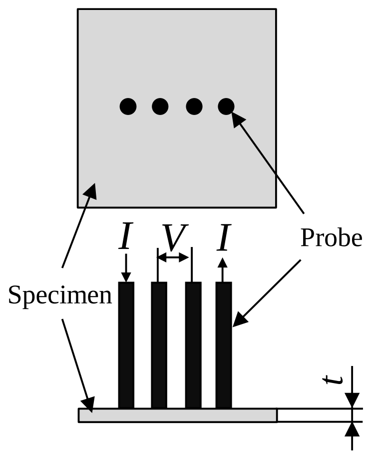

Figure 6: Schematic view of the method for measuring resistivity in the four-point probe method for energy director.

3 RESULTS AND DISCUSSION

3.1 Effects of CNT addition on welding behavior

In this experiment, the effects of adding CNT/PPS energy directors on welding behavior was investigated through ultrasonic welding. The energy directors used were PPS-ED (PPS polymer only), SWCNT/PPS-ED (PPS polymer energy with 1.0 wt% SWCNT), and MWCNT/PPS-ED (PPS polymer with 1.0 wt% MWCNT). Fig.7 shows fracture surface images where the ultrasonic welding process was stopped at every 0.3s. In the case of t_{UW}=0.3 s oscillation, melt spots were formed locally at the top of the resin pocket of the woven-CF/PPS laminate and the corresponding location in the energy director. Subsequently, at 0.6 s oscillation, the resin melting area expanded from the melting spots. At t_{UW}=0.9 s oscillation, the resin melting area grew over the entire joint area. When oscillation was performed for t_{UW}=1.2 s or more extended, resin melting progressed further, and the fiber bundles and matrix of the woven CF/PPS laminate flowed out of the welding surface. Fiber bundle deformation and void formation were also observed.

Fig.8 shows the effects of ultrasonic oscillation time on welding area ratio using PPS-ED, SWCNT/PPS-ED, and MWCNT/PPS-ED. The addition of SWCNT or MWCNT resulted in an increased melt area ratio compared to PPS-ED at an oscillation time of 0.3 s to 0.6 s. This is likely because of improved thermal conductivity and promotes polymer melting by adding CNT.

		Ultrasonic oscillation time, t_{UW} [s]					
		0	0.3	0.6	0.9	1.2	1.5
PPS-ED	Surface image	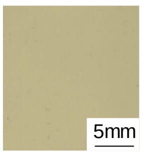	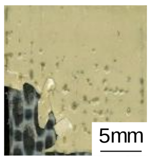	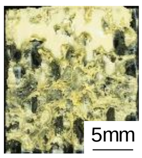		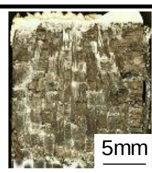	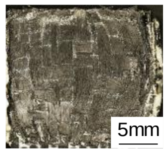
	ΔA_w[%]	0	13.7	86.0	100	100	100
SWCNT/PPS-ED	Surface image		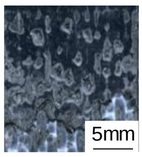	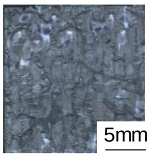	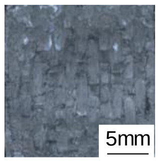	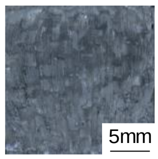	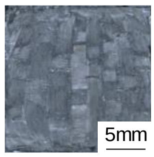
	ΔA_w [%]	0	27.2	94.9	100	100	100
MWCNT/PPS-ED	Surface image	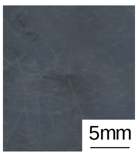		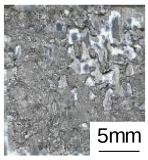	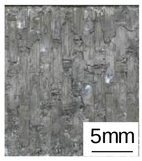	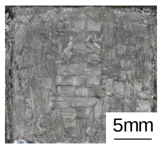	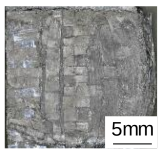
	ΔA_w [%]	0	20.1	92.7	100	100	100

Figure 7: Fracture surface images of ultrasonic welding part at various oscillation times using PPS-ED, SWCNT/PPS-ED, and MWCNT/PPS-ED. The welding area was increased with increasing the ultrasonic welding time.

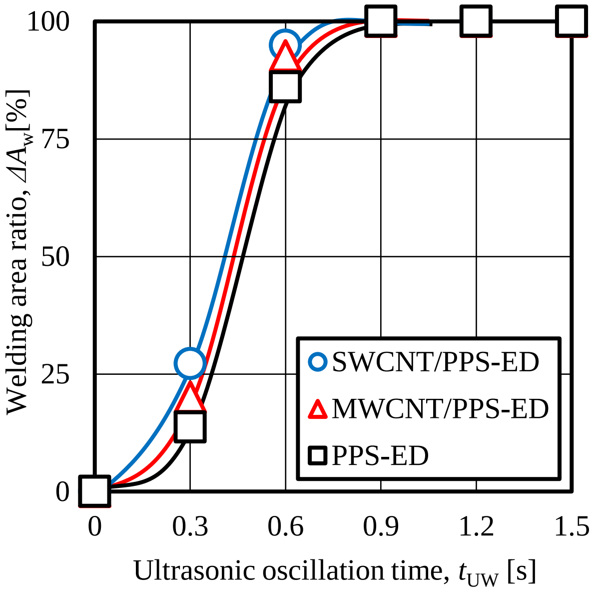

Figure 8: Effects of CNT addition on welding area ratio.

3.2 Effects of CNT addition on joining strength

In order to investigate the effect of the weight content of each CNT on single lap shear strength, woven-CF/PPS laminates were welded using PPS-ED, SWCNT/PPS-ED, and MWCNT/PPS-ED by the ultrasonic welding process. In this section, the CNT addition conditions of SWCNT/PPS-ED and MWCNT/PPS-ED were W_{CNT} = 0.1, 0.5, 1.0, 1.5, and 2.0 wt%. Fig.9 shows the effects of the weight content of CNT on single lap shear strength. In the case of MWCNT/PPS-ED, the single lap shear strength was increased by the addition of 0.5 wt% and 1 wt% MWCNT. The average single lap shear strength without CNT was 35.7 MPa. However, the single lap shear strength decreased gradually with the increase in the amount of SWCNT added. This suggests being due to stress concentration at the welding interface because of the agglomeration of SWCNT.

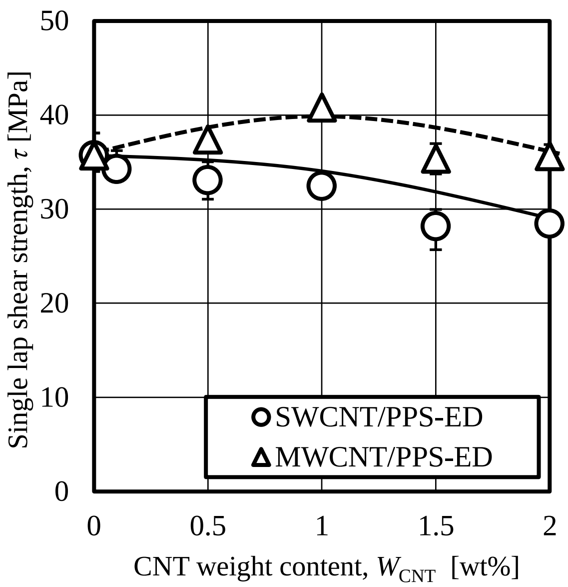

Figure 9: Effects of SWCNT and MWCNT weight content of energy director on single lap shear strength.

Fig.10 shows SEM images of fracture surface on the test specimens which were welded by ultrasonic welding using SWCNT/PPS-ED and MWCNT/PPS-ED. From SEM images, it was observed aggregation of CNT nano-networks in SWCNT/PPS-ED, but it was difficult to observe CNT in MWCNT. Because MWCNT aspect ratio is much smaller than that of SWCNT. From these results, the aggregation of SWCNT at the interface is considered to be the cause of the decreased interfacial joining strength with the polymer and the occurrence of stress concentration.

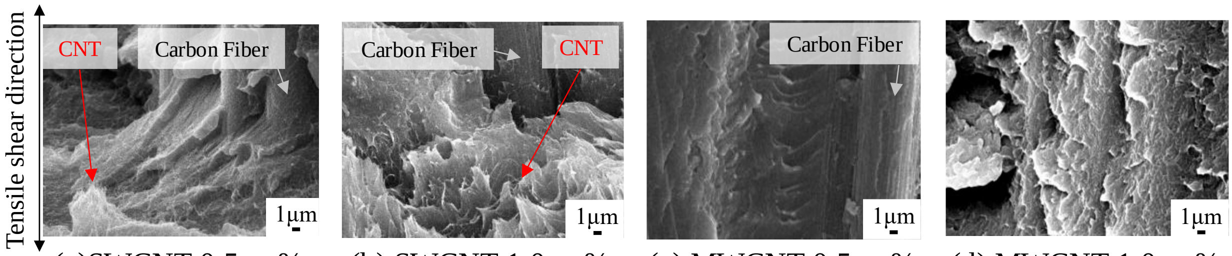

(a)SWCNT 0.5 wt% (b) SWCNT 1.0 wt% (c) MWCNT 0.5 wt% (d) MWCNT 1.0 wt%

Figure 10: SEM images of fracture surface at various SWCNT or MWCNT weight content.

3.3 Effects of CNT dispersion in energy director on volume resistivity and joining strength

In order to achieve both the maintain high joining strength and the structural health monitoring. of ultrasonic welding, we propose hybrid addition of MWCNT and SWCNT. Energy directors were prepared by mixing PPS polymer with SWCNT and MWCNT at weight ratios of 10:0, 9:1, 7.5:2.5, 5:5, 2.5:7.5, 1:9, and 0:10, with a total weight fraction of CNT at 0.5 and 1.0 wt%. SEM images of the fractured surfaces of energy directors with SWCNT and MWCNT under different ratios are shown in Fig.11. A comparison between the case of a 10:0 ratio (only SWCNT) and the case of a 9:1 ratio reveals a highly uniform dispersion of CNT in the 9:1 ratio. On the other hand, as the addition ratio of MWCNTs increases, the contact point of the CNTs decreases, suggesting a negative effect on sensing. To quantitatively evaluate the dispersion, the volume resistivity of energy directors with varying CNT addition ratios was measured at a total weight content of CNT at 0.5 wt%.

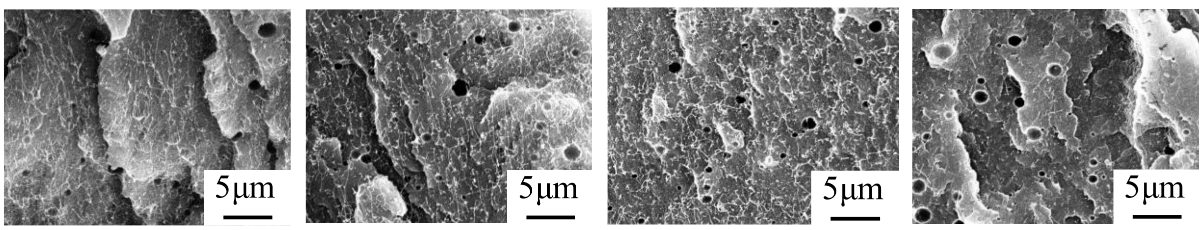

(a)CNT weight ratio 10:0 [SWCNT:MWCNT] (b)CNT weight ratio 9:1 [SWCNT:MWCNT] (c)CNT weight ratio 5:5 [SWCNT:MWCNT] (d)CNT weight ratio 1:9 [SWCNT:MWCNT]

Figure 11: SEM images of fractured surfaces of energy director at various weight ratios of SWCNT to MWCNT.

Fig.12 shows the volume resistivity and model diagram that was considered from SEM images of the fracture surface of the energy director. The volume resistivity of the case with 10:0 ratio was about 1000 [Ω·cm]. On the other hand, in the 9:1 case, the volume resistivity decreased to about one-tenth of that in the 10:0 case. This phenomenon can be attributed to the suppression of aggregation and the facilitation of conductive path formed by the addition of MWCNT between SWCNT, as illustrated in the model diagram Fig.12. As the MWCNT ratio increased, the volume resistivity also increased. However, when the ratios reached 2.5:7.5, 1:9, and 0:10, the resistance exceeded the measurement range, making it impossible to measure. It is suggested that as the addition ratio of MWCNT with a smaller aspect ratio than SWCNT increased, it became difficult to achieve isolated dispersion and form conductive paths, which becomes a disadvantage in sensing.

When the positions of CNTs in the polymer matrix form a conducting network, the conductivity of composite sharply increases. This phenomenon is known as percolation and can be well explained by percolation theory. So, the dispersion of CNT and electrical contacts between CNT in PPS polymer can be quantitatively evaluated using percolation theory. Fig.13 shows comparison of the effect of two types of CNT/PPS composites addition ratio (10:0 and 9:1) on the electrical resistivity as a function of CNT weight content. The results show that the percolation threshold is shifted toward the lower CNT weight content when the hybrids are added at a ratio of 9:1 rather than 10:0.

Therefore, it was concluded that the best dispersion was achieved by the hybrid addition of SWCNT and MWCNT at a 9:1 ratio in PPS polymer.

To investigate the effects of hybrid addition of SWCNT and MWCNT on single lap shear strength, energy directors were prepared using different weight ratios of SWCNT and MWCNT (10:0, 9:1, 7.5:2.5, 5:5, 2.5:7.5, 1:9, and 0:10) to achieve a total weight content of 0.5 wt% and 1.0 wt%. These energy directors were then used for ultrasonic welding of test specimens. Fig.14 shows the effects of SWCNT and MWCNT hybrid addition of energy directors on single lap shear strength. In the 10:0 case, single lap shear strength was the lowest among all weight ratios. From ratios of 9:1 to 1:9, single lap shear strength improved compared to 10:0, reaching values equivalent to the average single lap shear strength of 35.7 MPa observed in PPS-ED. This suggests that the entanglement of SWCNT and MWCNT may prevent re-aggregation during the welding process. Therefore, it is possible that a uniformly CNT network is maintained in the welding area, making the hybrid addition of CNTs beneficial for achieving CNT networks. This is particularly advantageous for sensing.

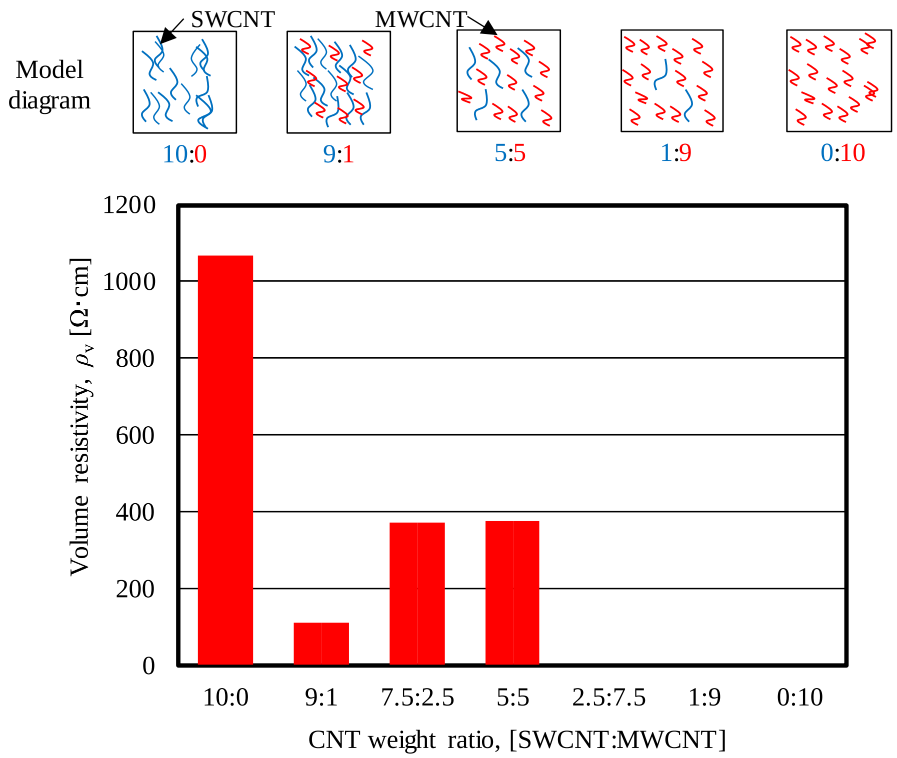

Figure 12: Comparison of the effect of CNT addition ratio on the volume resistivity of energy director.

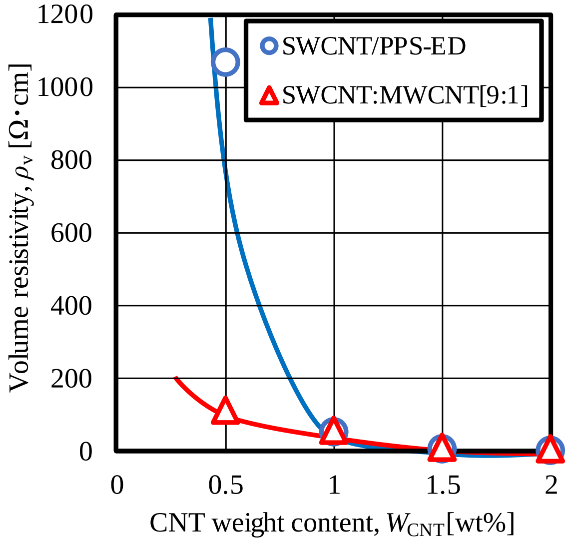

Figure 13: Electrical volume resistivity of two types of CNT/PPS composites as a function of CNT weight content.

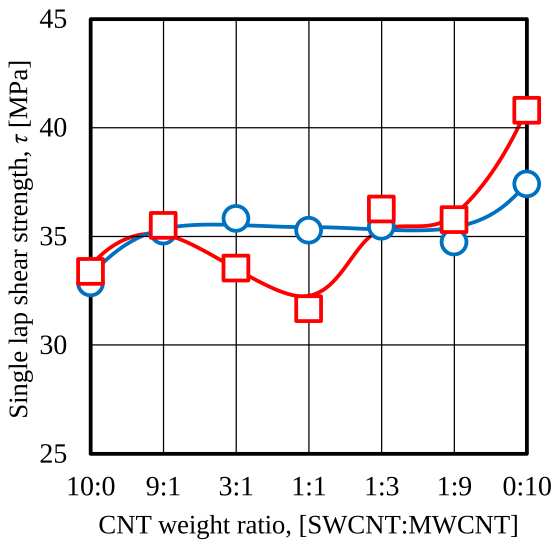

Figure 14: Effects of SWCNT and MWCNT hybrid addition of energy directors on single lap shear strength.

3.4 Self-sensing response of welded part

The experimental conditions were using energy directors with PPS-ED, SWCNT/PPS-ED (1.0 wt%), MWCNT/PPS-ED (1.0wt%), and SWCNT/MWCNT/PPS-ED (CNT weight ratio 9:1, [SWCNT:MWCNT], Total 1.0wt%). The specimens were welded with condition of displacement of δ=25 %. The tensile load obtained from the universal testing machine until fracture, initial resistance R_0 [Ω], and the resistance change behavior obtained from the digital multimeter are shown in Figure 15. It was observed that the resistance change followed the increase in load and strain for all conditions. Moreover, just before fracture, a rapid increase in resistance change was observed. This can be attributed to a reduction in the conductive path between the electrodes due to delamination or damage in the welding layer. Monitoring the slope of the resistance change could potentially be applied to predicting damage and fracture in the future. For the CNT 0 wt% condition, the resistance change rate was the highest. In particular, it exhibited a significant change rate of over 1000% at the moment of fracture. This is likely due to incomplete full melting of the welding area, resulting in a higher initial resistance R_0 compared to other conditions and capturing delamination and damage in the welding area more prominently. In the using SWCNT/PPS-ED and SWCNT/MWCNT/PPS-ED condition, smoother resistance change behavior was observed. It seems that a conductive network is formed by CNTs in the matrix from 3.3, and the piezoelectric effect is a major contributor to the conductivity.

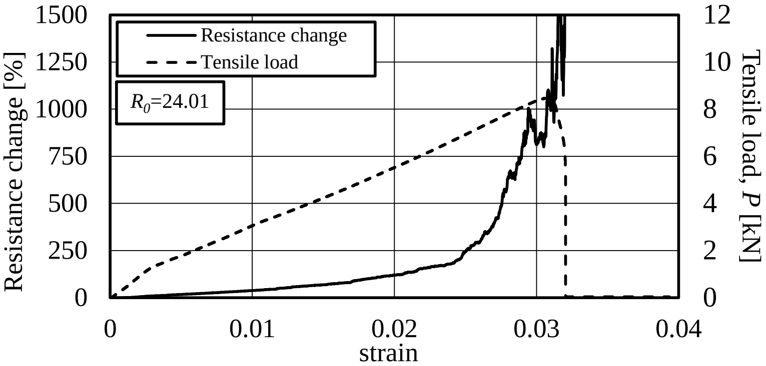

(a) PPS-ED(W_{CNT}=0 wt%)

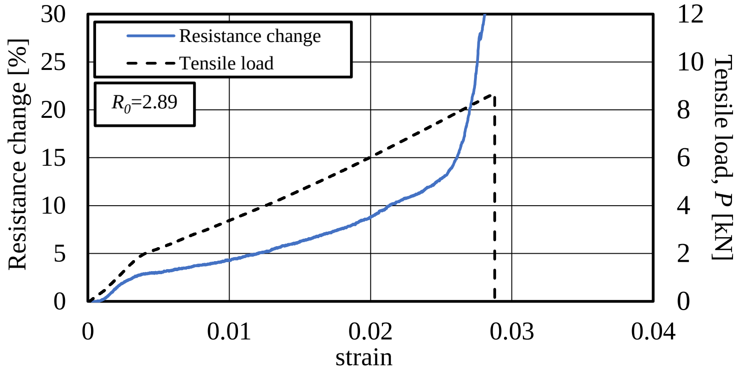

(b) SWCNT/PPS-ED (W_{CNT}=1.0 wt%)

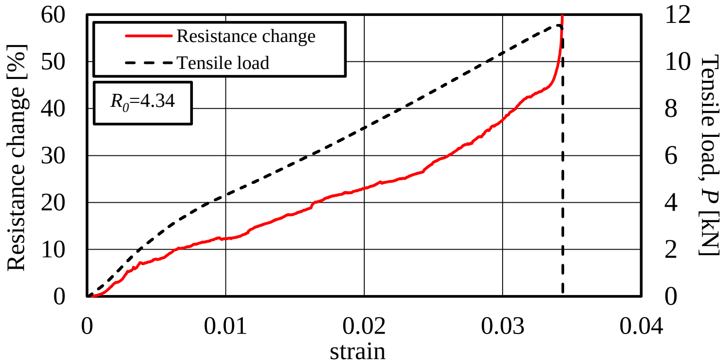

(c) MWCNT/PPS-ED (W_{CNT}=1.0 wt%)

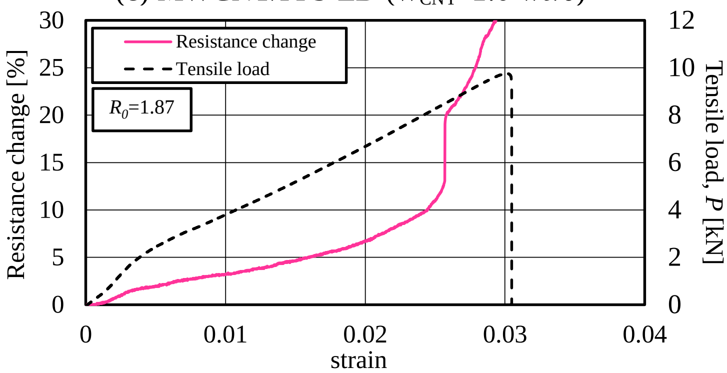

(d) SWCNT/MWCNT/PPS-ED (CNT weight ratio 9:1, [SWCNT:MWCNT], W_{CNT}=1.0wt%)

Figure 15: Load-strain and electric resistance changing rate curve of welded part.

4 CONCLUSIONS

This study aims to develop the ultrasonic welding process using carbon nanotube (CNT) added energy director to reveal the ultrasonic welding behavior, single lap shear strength, and functionality of welding part. The main conclusions are drawn as follows:

(1) In the case of using the CNT/PPS-ED as energy director, the welding area ratio was increased significantly compared to PPS-ED due to increasing thermal conductivity by addition CNT.

(2) The single lap shear strength increased in the case of the addition of 0.5 wt% MWCNTs, compared to the case of without CNTs. However, the single lap shear strength decreased gradually with the increase in the amount of SWCNT added, although SWCNTs constitute a network required for sensing.

(3) Hybrid addition of SWCNT and MWCNT to PPS polymer in a ratio of 9:1 was shown to result in uniform dispersion, suggesting that the use of SWCNT as energy director can be used to achieve both the maintain high joining strength and the structural health monitoring.

(4) From the result of the structural health monitoring, it was observed that the resistance change followed the increase in load and strain. Moreover, just before fracture, a rapid increase in resistance change was observed.

REFERENCES

[1] A. Köver, Simulation and Manufacturing of an Automotive Part for Mass Production, *Proceedings of 2nd International Conference and Exhibition on Thermoplastic Composites (ITHEC2014)*, A-3, pp.21-25, 2014.

[2] I.F. Villegas and G. Palardy, A comparative evaluation between flat and traditional energy directors for ultrasonic welding of CF/PPS thermoplastic composites, *Composite Interfaces*, Vol.24, No.5, pp.515-528, 2017.

[3] J.C. Yan, X.L. Wang, R.Q. Li, H.B. Xu and S.Q. Yang, The effects of energy director shape on temperature field during ultrasonic welding of thermoplastic composites, *Key Engineering Materials*, Vol.353-358, pp.2007-2010, 2007.

[4] E. Akay, F. Köhler, and I.F. Villegas, In-situ monitoring of weld line thickness in continuous ultrasonic welding of thermoplastic composites, *Proceedings of the 20th European Conference on Composite Materials (ECCM20)*, Vol.2, 2022.

[5] J.C. Abry, S. Bochard, A. Chateauminois, M. Salvia and G. Giraud, In situ detection of damage in CFRP laminates by electrical resistance measurements, *Composites Science and Technology*, Vol.59, No.6, pp.925-935, 1999.

[6] A. Todoroki, D. Haruyama, Y. Mizutani, Y. Suzuki and T. Yasuoka, Electrical resistance change of carbon/epoxy composite laminates under cyclic loading under damage initiation limit, *Open Journal of Composite Materials*, Vol.4, No.1, 2014.

[7] W. Li, H. Frederick, G. Palardy, Multifunctional films for thermoplastic composite joints: Ultrasonic welding and damage detection under tension loading, *Composites Part A: Applied Science and Manufacturing*, Vol. 141, 2021.

[8] T. Bregar, D. An, S. Gharavian, M. Burda, I. Durazo-Cardenas, V.K. Thakur, D. Ayre, M. Słoma, M. Hardiman, C. McCarthy and H. YazdaniNezhad, Carbon nanotube embedded adhesives for real-time monitoring of adhesion failure in high performance adhesively bonded joints, *Scientific Reports*, 10, 16833, 2020.

[9] Y. Buser, G. Bieleman, W. Grouve, S. Wijskamp and R. Akkerman, Self-powered structural health monitoring of novel thermoelectric energy harvesting GFRP composites, *Proceedings of the 20th European Conference on Composite Materials (ECCM20)*, Vol.3, pp.83-91, 2022.

[10] M. Surgeon and M. Wevers, The influence of embedded optical fibres on the fatigue damage progress in quasi-isotropic CFRP laminates, *Journal of Composite Materials*, Vol.35, pp.931-940, 2001.